SAE INTERNATIONAL

ARTICLE INFO

Article ID: 09-11-03-0013

doi:10.4271/09-11-03-0013

Thermal Modeling of the Electric Vehicle Fire Hazard Effects on Parking Building

Andrii Gavryliuk,[1] Roman Yakovchuk,[1] Yaroslav Ballo,[2] and Yuriy Rudyk[1]

[1]Lviv State University of Life Safety, Ukraine
[2]The Institute of Public Administration and Research in Civil Protection, Ukraine

Abstract

The world community is constantly and rapidly moving toward the search for alternative and ecologically clean energy sources, including for transport, and Russia's war against Ukraine only intensified and accelerated such processes. This trend in transport is reflected in the spread of battery-powered electric vehicles (BEVs) with zero emission of harmful gases.

Electric cars are experiencing a rapid increase in numbers, accompanied by the emergence of lesser-known risks. Among these hazards are the occurrence of fires in electric vehicles, primarily caused by component failures, notably the widely prevalent lithium-ion batteries.

Fires of such cars have a different character compared to fires of vehicles powered by an internal combustion engine vehicle (ICEV). In this study, using the fire dynamics simulator developed by the National Institute of Standards and Technology, a BEV fire was simulated on the example of the Tesla Model S. For this, a description of the objects and their physical characteristics were carried out, the input parameters of the BEV and environmental parameters were set, and a mathematical model of the development dynamics of fire was formed. According to the modeling results, it was found that the minimum fire protection distance from a BEV to the wall of buildings of various functional purposes should be at least 3 m, provided that the free fire development time is 600 s.

History

Received: 02 May 2023
Revised: 31 Jul 2023
Accepted: 17 Aug 2023
e-Available: 21 Sep 2023

Keywords

Fire of electric vehicle, Battery failures, Electric vehicle parking, Fire hazard, Lithium-ion battery

Citation

Gavryliuk, A., Yakovchuk, R., Ballo, Y., and Rudyk, Y., "Thermal Modeling of the Electric Vehicle Fire Hazard Effects on Parking Building," *SAE Int. J. Trans. Safety* 11(3):2023, doi:10.4271/09-11-03-0013.

ISSN: 2327-5626
e-ISSN: 2324-5634

1. Introduction

The world car fleet has more than 1 billion vehicles, and according to forecasts, their number will increase to 2.5 billion within 50 years [1]. Such trends sharply outlined the issue of environmental safety and EV can contribute to decreasing negative environmental effects. The very idea of electric cars originated in the 1800s [2].

According to [3], the share of electric vehicles in 2021 exceeded 10% of global car sales and continues to grow. The total number of operated electric vehicles as of the end of 2022 is almost 27 million (Figure 1).

The majority of such vehicles are concentrated in China, Europe, and the United States, with passenger vehicles and buses being the most common.

As their service life increases, the number of their fires is predicted to increase as well.

A source of electrical energy is used to power the electric motors of electric vehicles. Today, lithium-ion batteries (LIB) are the most widely used. They are widely recognized as advanced energy storage systems (ESS) due to their increased capacity, high charge–discharge efficiency, and extended lifetime. Under certain conditions, chemical and electrophysical processes lead to an uncontrolled exothermic reaction. Such reactions lead to the release of harmful and dangerous gases [4], ignition, and explosions, which are often accompanied by fire and cause not only material damage but also human casualties [5, 6, 7].

There are various types of LIB used in electric vehicles, including $LiCoO_2$, $LiMn_2O_4$, $LiNiMnCoO_2$, $LiNiCoAlO_2$, and the like, the fire hazards of which is given in [8].

Electric vehicle fires and explosions [9, 10, 11, 12] are a severe concern for consumers and the public and create new challenges for the scientific community and for firefighters.

These scientific papers describe current research on security and risk assessment [13, 14]. The purpose of computational fluid dynamics (CFD) modeling is to identify the main thermodynamic parameters that occur during electric vehicle fires. Therefore, in this study, using the fire dynamics simulator developed by the National Institute of Standards and Technology, an EV fire was simulated on the example of a Tesla Model S. The features of the development and spread of fire, heat flows, temperatures, and the like, which occur as a result of electric vehicle fires, will create a basis for the study of holistic fire safety, both of the vehicles themselves and the development of construction requirements for various types of charging stations and parking lots and their fire protection systems.

The world scientific community pays a lot of attention to various types of research on LIB, including the modeling of processes that occur as a result of their failures. Most of the research is focused on the study of battery failures as a separate element. In scientific works [15, 16, 17], the processes of temperature change during the charging and discharging of LIB were studied. A group of researchers led by Abada, S. [18] summarized modeling approaches and perspectives to investigate the safety of LIB. A series of works by Anderson, J. and others [19, 20] investigated the spread of fire between elements of a lithium-ion battery, which was caused by thermal runaway propagation (TRP).

In works [21, 22, 23, 24, 25], models and temperature parameters of failures arising as a result of a violation of the rules of operation of LIB are described.

FIGURE 1 Dynamics for electric vehicle numbers in world regions.

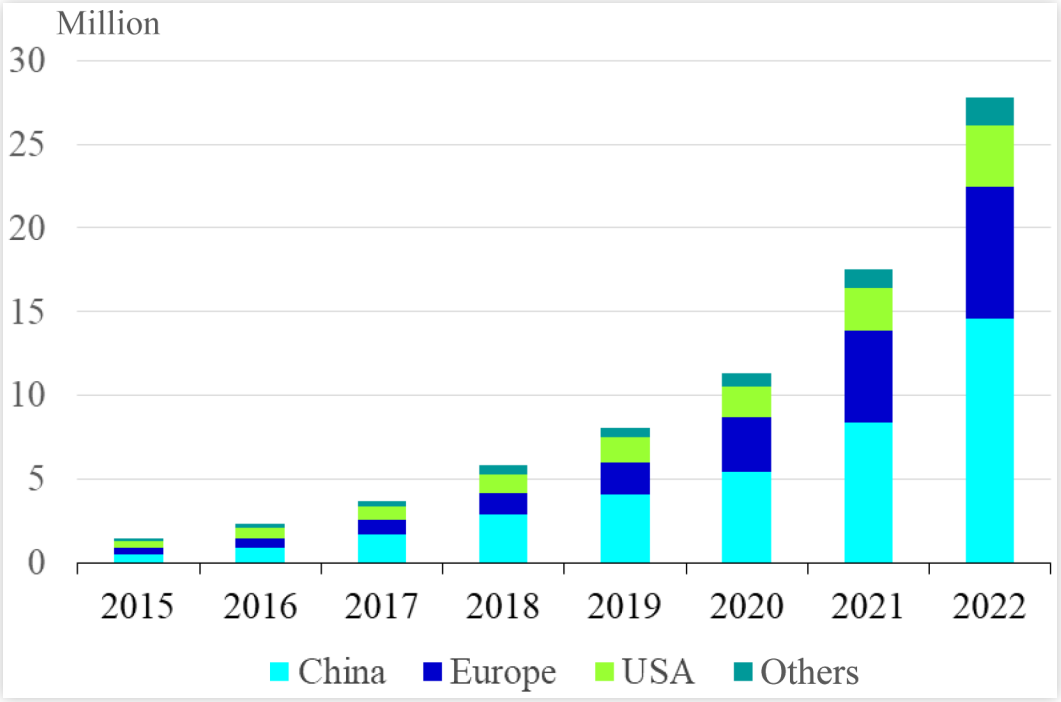

With the use of CFD, works [22, 23] investigated the gases released due to the TRP of LIB and also described their explosion parameters, such as the explosion pressure and the speed of the flame front.

The estimation of the temperature of LIB during the charging process is given in [26].

An outline of the dangers of car fires and a study of their causes are given in the work [27]. The study of malfunctions and welding defects of the exhaust manifold, which caused the car fire, is given in the work [28].

Researchers Xiao, M. and Choe, S. Y. [29] developed a calorimeter to dynamically measure the heat from a power cell, which allowed the heat generation equation to be refined.

In [30], the influence of the ambient temperature, the discharge rate of the $LiFePO_4$-type battery, as well as its geometric dimensions on the release of heat during the operation was investigated.

Rashidi [31] and others have thoroughly investigated temperature control methods in fuel cells and supercapacitors used in electric vehicles together with LIB.

The work [32] examines the mechanical integrity of LIB packages of electric vehicles in order to ensure their operation under mechanical action. Ensuring the integrity of LIB packages during mechanical action prevents internal short circuit and electric vehicle fire.

Sascha Voigt [33] and others using the CFD software complex conducted fire tests of a lithium-nickel-manganese-cobalt-oxide battery with a total weight of 17 kg. The results show that the maximum temperature during the fire test is 800–850°C and is reached at 70–75 s from the start of the fire test, and the total heat flow is 1.75 MW at 65–75 s from the start of the test.

The paper [34] examines the influence of various types of mechanical load on LIBs of electric vehicle on the probability of short circuit and thermal runaway.

Yih-Wen Wang and Chi-Min Shu [35] conducted a thorough and up-to-date review of the mechanism of thermal energy production in exothermic reactions in LIB.

In return, much less attention has been paid to the fire research of electric vehicles compared to the research on individual battery failures.

It is obvious that the fires of electric cars have a different character than the fires of cars with internal combustion engines. This is due to the lack of fuels and lubricants such as gasoline, diesel, or LPG, as well as various combustible lubricants and other materials.

In work [24], a fire in the tunnel of a truck with LIB, in the amount of 100 units, each of which has a mass of 250 kg (the batteries are transported as cargo), was investigated. The curve of thermal radiation from a battery fire reaches its peak 30 minutes after the start of the fire test and is 140 MW, which exceeds the value of the curve of thermal radiation from the burning of flammable goods.

Feng, X. et al. [36] summarized the dangers and the process of the occurrence of exothermic reactions in electric vehicle batteries and also considered ways to prevent the occurrence of such a failure. However, the hazard was considered only on the scale of the batteries, not the electric vehicle as a whole.

Obviously, full-scale fire tests require large financial outlays, but such tests are carried out. Initially, these were tests on cars with internal combustion engines [37, 38, 39, 40, 41]. Later, scientific works appeared in which electric vehicle fires were investigated [42, 43, 44, 45].

The value of electric vehicle fire tests is the experimental study of such key parameters as the total amount of thermal energy released (J), the rate of thermal energy release (J/s), the power of thermal radiation (W/m^2), and others. Understanding the dynamics of such key parameters, which arise as a result of electric vehicle fires, will allow the creation of standards and regulations, as they would apply to both building structures and other infrastructure of the use of electric vehicles.

Sungwook Kang et al. [46] conducted full-scale fire tests of BEVs, ICEVs, and FCEVs. The BEVs were equipped with LIB of 39 and 64 kWh each and fully charged. And the FCEV is equipped with a battery capacity of 1.56 kWh. Ignition was initiated using a propane burner and an electric heater with a power of 575 W. The authors established that the power of heat release for BEV was about 7.25 MW/m^2, and the total energy of heat release was 9 GJ. For ICEV, the heat generation capacity was 7.66 MW/m^2 and a total of 8 GJ. The FCEV combustion was characterized by a lower heat release capacity of 5.99 MW/m^2, but the total heat release was the largest—10.82 GJ. And the peak power of thermal radiation for BEV was in the range of 40–60 kW/m^2 at the height of 227 cm above BEV during 30–40 minutes from the start of the fire test, and temperatures exceeded 900°C. At the same time, the authors found that the specific heat of combustion for BEVs is more than 30 MJ/kg. This indicator is 45.9 MJ/kg for LIB, which is comparable to the heat of combustion of flammable liquids such as gasoline and diesel fuel.

Willstrand et al. [47] conducted fire studies of BEVs and ICEVs, and the heat release rate (HRR) for both vehicles was similar, but the HRR for the 1 MW BEV was greater than for the ICEV.

Sturm, P. et al. [48] conducted full-scale fire tests for EVs and ICEVs in tunnels. And for two identical SUVs, one powered by a diesel ICE engine and the other powered by an 80 kWh NMC battery at 100% state of charge (SOC), the HRR was significantly different. For the ICEV, the maximum HRR was almost 5 MW at 1100 s from the start of the fire test, and for the EV, it was more than 10 MW at 900 s from the start, confirming a more dynamic fire development.

2. Research and Methodology Purpose

The purpose of this study is to substantiate the safe firefighting distances of electric vehicles and adjacent objects for parking lots and closed garages using the fire dynamics simulator (FDS) [49, 50], modeling the thermal effect on adjacent objects in the event of an electric vehicle fire.

The verification and validation of the calculation method are carried out based on the principles of the international standard [51].

During the application of FDS modeling, it is intended to determine the possible temperature impact from an electric car fire at the place of its charging in the parking lot adjacent to the adjacent building. In particular, during the calculation, the possibility of the shielding property of the adjacent wall should be taken into account as the most unfavorable scenario for the development of fire in open parking lots.

2.1. Description of the Calculation Method and Formation of a Mathematical Model of Fire Development Dynamics

The simulation of fire dynamics is carried out using the FDS computer program developed by the National Institute of Standards and Technology (NIST, USA) [49, 50, 52].

The FDS program simulates fire scenarios using a CFD model optimized for low-velocity temperature-dependent flows. This approach is very flexible and can be applied to various fires, ranging from furnace fires to oil tanker fires. FDS implements a CFD model of heat and mass transfer during combustion and numerically solves the Navier–Stokes equation for low-speed temperature-dependent flows, with particular attention paid to smoke propagation and heat transfer during a fire. The main algorithm is a specific scheme of the predictor–corrector method of the second order of accuracy in terms of coordinates and time. Turbulence is performed using Smagorinsky's large-scale Eddy simulation (LES) model. Direct numerical simulation (DNS) can be performed if the underlying grid is sufficiently accurate. Large-scale simulation of vortices is the default mode of operation [52].

In most cases, FDS uses a one-step chemical reaction. Its results are transmitted through a two-parameter mixture fraction model. "Mixture fraction," as used herein, is a scalar quantity that gives the mass fraction of one or more gas components at a given point in the flow. By default, two components of the mixture are calculated: the mass fraction of unburned fuel and the mass fraction of burned fuel (i.e., combustion products). A two-stage chemical reaction with a three-parameter decomposition of a particle in the mixture is divided into one-stage reactions—oxidation of fuel to carbon monoxide and oxidation of monooxyl to dioxide. In this case, there are three components: the unburned fuel, the mass of fuel that completed the first step of the reaction, and the mass of fuel that completed the second step of the reaction. The mass concentration of all major reactants and products can be obtained using the "state ratio." It is also possible to use a multistep reaction with a finite flow rate [52].

Radiative heat transfer is included in the model by solving the radiative transfer equation for the ideal gas and, for some limited cases, using a broad-band model. The equation is solved using a method similar to the control volume method for convective transfer (FVM). Soot and smoke absorption coefficients were calculated using the RADCAL narrowband model. FDS geometry solves the governing equations on a rectangular grid. Obstacles must be rectangular to satisfy grid parameters.

For all solid surfaces, thermal boundary conditions are set, including data on the flammability of the material. Heat and mass transfer from the surface and back is calculated using empirical ratios [53].

A special SmokeView program is used to display and visualize the simulation results of the FDS program.

During the formation of the mathematical model of the dynamics of fire development, the following mathematical dependencies were used. In its usual form, the system of Navier–Stokes equations [50] consists of two equations: the equation of motion and the equation of continuity.

In vector form for an incompressible fluid, they are written as follows:

$$\frac{\partial \rho}{\partial t} + \nabla(\rho V) = 0 \qquad \text{Eq. (1)}$$

$$\frac{\partial}{\partial t}(\rho V) + \nabla[\rho V \otimes V] = -\nabla p + \nabla\left[(\mu + \mu_t)\left(\nabla V + (\nabla V)^{\mathrm{T}}\right)\right] + S \qquad \text{Eq. (2)}$$

$$\frac{\partial}{\partial t}(\rho h) + \nabla(\rho V h) = \nabla\left(\left(\frac{\lambda}{c_p} + \frac{\mu_t}{\mathrm{Pr}_t}\right)\nabla h\right) + Q_{rad} \qquad \text{Eq. (3)}$$

$$\frac{\partial}{\partial t}(\rho Y_k) + \nabla(\rho V Y_k) = \nabla\left(\left(\frac{\mu}{\mathrm{Sc}} + \frac{\mu_t}{\mathrm{Sc}_t}\right)\nabla Y_k\right) + Q_k \qquad \text{Eq. (4)}$$

where t is time; ρ is density; V is the relative velocity vector; p is relative pressure; μ is molecular dynamic viscosity; μ_t is turbulent dynamic viscosity; λ is the thermal conductivity coefficient of the mixture; Pr_t is the turbulent Prandtl number; Sc is the Schmidt number; Sc_t is the turbulent Schmidt number; Y_k is the concentration of the kth component of the combustion reaction.

The static enthalpy h of the mixture is determined by the expression:

$$h = h_0 + \int_{T_0}^{T} c_p dT + \sum_k Y_k H_k \qquad \text{Eq. (5)}$$

where

T is temperature

h_0 is initial enthalpy at temperature T_0

$c_p = \sum_k Y_k c_{p,k}$ is heat capacity of the mixture at constant pressure

H_k is the heat of formation of the kth component

The initial term of Equation 2 S is determined by the expression:

$$S = \left(\rho - \rho_{hyd}\right)g + \rho B, \qquad \text{Eq. (6)}$$

where ρ_{hyd} is the hydrostatic density; g is the vector of gravitational forces; B is a vector of rotational forces (centrifugal and Coriolis), calculated according to the formula:

$$B = -2\omega \times V, \qquad \text{Eq. (7)}$$

where ω is the angular velocity vector.

To determine the turbulent viscosity, various options are used related to the methods of determining the mediated and fluctuating components of the quantities included in the Navier–Stokes equation. These methods of determining turbulent dynamic viscosity are called turbulence models. The standard k-ε turbulence model is the most widely used. According to this model, the dynamic, turbulent viscosity is determined by the expression:

$$\mu_t = C_\mu \rho \frac{k^2}{\varepsilon} \qquad \text{Eq. (8)}$$

where $C_\mu = 0.09$ is a constant coefficient; ε is the dissipation rate of turbulent energy; k is turbulent energy.

To determine the values of ε and k, equations are used that complement the system of Navier–Stokes equations, which have the form:

$$\frac{\partial(\rho k)}{\partial t} + \nabla(\rho V k) = \nabla\left(\left(\mu + \frac{\mu_t}{\sigma_k}\right)\nabla k\right) + \mu_t G - \rho\varepsilon \qquad \text{Eq. (9)}$$

$$\frac{\partial(\rho\varepsilon)}{\partial t} + \nabla(\rho V \varepsilon) = \nabla\left(\left(\mu + \frac{\mu_t}{\sigma_\varepsilon}\right)\nabla\varepsilon\right) + C_1 \frac{\varepsilon}{k}\mu_t G - C_2 f_1 \rho \frac{\varepsilon^2}{k} \qquad \text{Eq. (10)}$$

where G is the value determined by the expression:

$$G = D_{ij}\frac{\partial V_i}{\partial x_j} \qquad \text{Eq. (11)}$$

where the D_{ij} value is defined as

$$D_{ij} = S_{ij} - \frac{2}{3}\left(\nabla \cdot \mathbf{V} + \frac{\rho k}{\mu_t}\right)\delta_{ij} \qquad \text{Eq. (12)}$$

The value δ_{ij}, which is included in Equation 2, is defined as:

$$S_{ij} = \frac{\partial V_i}{\partial x_j} + \frac{\partial V_j}{\partial x_i} \qquad \text{Eq. (13)}$$

Other parameters included in Equations 2 and 3 are constant.

To close the system of Equations 1–4, the equation of the state of an ideal gas is used. For a mixture of gases, it is written in the form:

$$p = \rho R_0 T \sum_k \frac{Y_k}{M_k} \qquad \text{Eq. (14)}$$

where R_0 is the universal gas constant; M_k is the molar mass of the kth component.

Equations describing combustion in a two-phase flow of air and liquid fuel particles. Combustion is represented by the generalized chemical hydrocarbon formula $C_xH_yO_z$ (C_6H_6O). The heat of combustion of liquid fuel (LHV) is determined by the following formula:

$$\mathrm{LHV}_{liq,fuel} = h^0_{liq,fuel} - h^0_{CO_2}\frac{44x}{12x + y + 16z} - h^0_{H_2O}\frac{9y}{12x + y + 16z} \qquad \text{Eq. (15)}$$

where

$h^0_{liq,fuel}$, $h^0_{CO_2}$, $h^0_{H_2O}$ are heats of formation, carbon dioxide, and water

x, y, z are stoichiometric coefficients for kerosene, equal to 6, 6, and 0, respectively

The gas phase is a mixture of five gases, therefore the primary system (1)–(4) is supplemented with five more equations for each of the components of the gas mixture: volatile $C_xH_yO_z$, O_2, N_2, H_2O, and CO_2, which have the form:

$$\frac{\partial}{\partial t}\left(\rho Y_k\right) + \nabla\left(\rho V Y_k\right) = \nabla\left(\left(\rho D_i + \frac{\mu_t}{\mathrm{Sc}_t}\right)\nabla Y_k\right) + Q_i^P + Q_i^{chem}, \qquad \text{Eq. (16)}$$

where the initial Q_i^{chem} term is equal to the gas-phase combustion gross reaction rate for the first volatile equation, for the others it is equal to zero.

The initial terms of the mixture components for the main equations of the system (1)–(4) are determined by the expressions:

$$Q_i^P = \sum_j \left(m_{i,in} - m_{i,out}\right)_j \frac{N_{pj}}{\Omega_{cell}} \qquad \text{Eq. (17)}$$

$$\bar{Q}_{mom}^P = \sum_j \frac{\pi r_p^2}{2} C_{Dj}\rho_g \left|V_g - V_p\right|\left(V_g - V_p\right)_j \frac{N_{pj}}{\Omega_{cell}} \qquad \text{Eq. (18)}$$

$$Q_{enth}^P = \sum_j \left(m_{i,in}h_{i,in} - m_{i,out}h_{i,out}\right)_j \frac{N_{pj}}{\Omega_{cell}} \qquad \text{Eq. (19)}$$

where the index i refers to the gas component; index j to the corresponding trajectory of the particle; N_{pj} is the number of particles passing through the trajectory per second; Ω_{cell} is the volume of the computational cell; C_{Dj} is the resistance coefficient of the particles flying along the trajectory; ρ_g is the gas-phase density; r_p is the radius of the particle.

The combustion model is also determined by the consumption of fuel, oxidizer, and combustion products.

Quantitative ratios are determined by the generalized chemical equation:

$$C_xH_yO_z + \left(x + 0.25y - 0.5z\right)O_2 \xrightarrow{W} CO_2 + 0.5yH_2O \quad \text{Eq. (20)}$$

The reaction rate W is determined by the stoichiometric coefficient:

$$Wi_{chem} = \frac{32\left(x + 0.25y - 0.5z\right)}{12x + y + 16z} \quad \text{Eq. (21)}$$

To account for radiant heat exchange in a gaseous medium and mutual heat exchange between the medium and particles, as well as a solid material, it is advisable to use the diffusion model of gas radiation (P1). This model is built on the assumption that the optical medium is isotropic, and the process of radiative heat transfer is described by the equation:

$$\nabla\left(\frac{1}{\alpha + \beta}\nabla E_r\right) + 3\left(\alpha E_b - \alpha E_r\right) = 0 \quad \text{Eq. (22)}$$

where E_r is the radiation energy density; E_b is the equilibrium radiation energy density determined by the equation:

$$\alpha E_b = \alpha_m E_{b,m} + \alpha_p E_{b,p} \quad \text{Eq. (23)}$$

α is the spectrum integral absorption coefficient:

$$\alpha = \alpha_m + \alpha_p \quad \text{Eq. (24)}$$

β is the scattering coefficient integrated over the spectrum:

$$\beta = \beta_m + \beta_p \quad \text{Eq. (25)}$$

In Equations 22–25, the quantities used have the following designations:

- α_m, α_p—absorption coefficients according to the gas medium and particles;
- β_m, β_p—scattering coefficients according to the gas medium and particles;
- $E_{b,m}$, $E_{b,p}$—the equilibrium radiation energy density for the gas phase and the phase of scattering particles, respectively, for the gas medium and particles.

The named quantities are determined by the formulas:

$$E_{b,m} = \sigma T_m^4 \quad \text{Eq. (26)}$$

$$\alpha_p E_{b,p} = \frac{1}{\Omega_{cell}}\sigma\varepsilon_p\sum_j \pi r_j^2 N_j T_{pj}^4 \quad \text{Eq. (27)}$$

$$\alpha_p = \frac{1}{\Omega_{cell}}\varepsilon_p\sum_j \pi r_j^2 N_j \quad \text{Eq. (28)}$$

$$\beta_p = \frac{1}{\Omega_{cell}}\left(2 - \varepsilon_p\right)\sum_j \pi r_j^2 N_j \quad \text{Eq. (29)}$$

where σ is the Stefan–Boltzmann constant; T_{pj} is the temperature of j—that particle; N_j is the number of particles in the cell; ε_p is the degree of particle blackness.

The initial term in Equation 1 is determined by equality:

$$Q_{rad} = -4\alpha n^2\left(E_b - E_r\right) \quad \text{Eq. (30)}$$

where n is the refractive index of the medium.

Considering the methods of numerical solution of the basic equations of the heat exchange model during fire tests of reinforced concrete slabs for fire resistance [49]. The basic Navier–Stokes system equations for this process can be written in the following generalized form:

- Equation of the diffuse type:

$$\frac{\partial}{\partial t}\left(TS \cdot f\right) = \frac{1}{PS}\nabla\left(DS \cdot \nabla f\right) + SST \quad \text{Eq. (31)}$$

- Equations of the diffusion–convection type:

$$\frac{\partial}{\partial t}\left(TS \cdot f\right) + \nabla\left(CC \cdot Vf\right) = \frac{1}{PC}\nabla\left(DC \cdot \nabla f\right) + SST \quad \text{Eq. (32)}$$

where the generalized values TC (time coefficient), CS (convective coefficient), PC (prediffusion coefficient), and DC (diffusion coefficient) determine the coefficients of the equation based on the corresponding derivatives, and the value SST (scalar source term) specifies the output term.

To integrate the generalized Equations 31 and 32, they are approximated for the discretizing domain by means of an adaptive locally fine mesh. The generalized equations approximated for the discrete area during the implementation of the implicit calculation scheme have the following form:

$$\frac{\left(TC \cdot f\right)^{n+1} - \left(TC \cdot f\right)^n}{\tau} = \frac{1}{TC}\nabla_h\left(DC \cdot \nabla_h f^{n+1}\right) + SST \quad \text{Eq. (33)}$$

$$\frac{\left(TC \cdot f\right)^{n+1} - \left(TC \cdot f\right)^n}{\tau}\nabla^{(k,s)}\left(CC \cdot VF^{n+1}\right) = \frac{1}{PC}\nabla_h\left(DC \cdot \nabla_h f^{n+1}\right) + SST \quad \text{Eq. (34)}$$

where

t is the time step

$TC \cdot f$ is difference approximation of the convective operator, with $k = 1$ (first order of accuracy), $s = 0$ (disregarded transfer through cell edges and vertices)

$\nabla_h(DC \cdot \nabla_h f^{n+1})$ is the difference approximation of the diffusion operator

2.2. Description of Calculated Objects and Their Physical Characteristics

During the simulation of temperature formations, it was assumed that the fire developed freely during the entire simulation time (720 s). The minimum duration of the simulation is based on the normative time of arrival of fire and rescue units at the scene of the fire (600 s), as well as taking into account the additional time (120 s) conditionally necessary for the deployment of forces and means.

During the creation of the BEV computer model, the model of the Tesla Model S electric car was taken as a basis, with dimensions of 4976 × 1963 × 1435 mm (length, width, height), with a total weight of 2100 kg. The choice of this type of electric vehicle is due to the largest capacity of the traction battery currently used among passenger electric cars, namely, the capacity of the battery is 104 kWh. The analysis of technical reports [54, 55] showed that it is extremely difficult to reproduce the complete design of LIB using FDS simulation; however, knowing the main components of the combustion reaction components of cathode materials, it is possible to accurately reproduce the temperature regime of the combustion reaction, which is the main task.

A lithium battery pack consists of various electrochemical components, including a cathode, anode, separator, and electrolyte. Each of them plays an important role in the properties of electric vehicle traction batteries in terms of specific energy, service life, safety, and cost. The type of cathode and anode material is often used to classify LIB into groups because their chemistry is one of the main variable properties in battery design.

Lithium cobalt oxide (LCO) is common in a large number of common household electronic devices, including smartphones. It provides relatively high power and voltage compared to other cathode materials and is relatively easy to manufacture. However, there are significant fire safety issues, especially when LIB are used at high temperatures or accidentally overcharged, and they have poor thermal stability. Thus, today manufacturers choose safer cathode materials such as lithium iron phosphate (LFP), lithium nickel, manganese cobalt oxide (NMC), lithium manganese oxide (LMO), or mixtures of different cathode materials.

The characteristics of cathode materials can be parametrically changed by mixing different cathode materials, and such materials are called hybrid or mixed cathode materials. To date, aluminum oxide (NCA) paired with graphite anodes are the most common cathode materials.

Field studies of combustion processes of LIB of electric vehicles showed [52] that the maximum temperature of free combustion of a battery that was artificially brought to an emergency mode with subsequent ignition during the period of the highest rate of heat release is 850–1020°C. At the same time, the total duration of free burning of the battery in most cases was at least 70 minutes.

Full-scale tests and studies of heat release from fires of EV and ICEV are presented in [53]. Analyzing this work shows that in the first 8–10 minutes, the combustion reaction has a low intensity, and therefore it is advisable to take into account the temperature regime that occurs in the period from 10 to 22 minutes, where the greatest intensity of heat generation is observed.

Separately, it should be noted that a study of fires of the same types of vehicles equipped with an electric engine and a gasoline engine showed that for a Nissan Leaf battery with a capacity of 24 kWh, the total value of heat release as a result of the fire was 0.9 GJ. For a similar type of car with a gasoline engine with a full fuel tank of 50 L, the total value of heat release as a result of the fire was 1.8 GJ.

For the Tesla S electric car under study, the total amount of heat released as a result of the fire was up to 3 GJ. Thus, when creating a model, you should focus on this highest value of heat release.

In addition to the battery, the fire load of the electric vehicle is rubber—118.4 kg (lower heat of combustion 33.52 MJ/kg); lubricants—8.4 kg (lower heat of combustion 41.87 MJ/kg); polymer materials—49.7 kg (lower heat of combustion 24.3 MJ/kg); polyurethane foam—32.6 kg (lower heat of combustion 47.14 MJ/kg); cellulose products—6.1 kg (lower heat of combustion 13.4 MJ/kg); artificial leather—14.2 kg lower heat of combustion (17.76 MJ/kg) [56, 57, 58, 59].

In Figure 2 a fragment of the reproduced FDS model that will be used in the study is given.

The selected fire scenarios are based on the presence of a wall structure made of red brick with the following physical characteristics: density 1950 kg/m^3; specific heat capacity 1.04 kJ/(kg · K); radiation coefficient 0.9; absorption coefficient 0.65 1/m.

Based on the given data and their physical characteristics, the main studied objects of the FDS model were created.

FIGURE 2 Visualization of the Tesla S electric car model created by FDS.

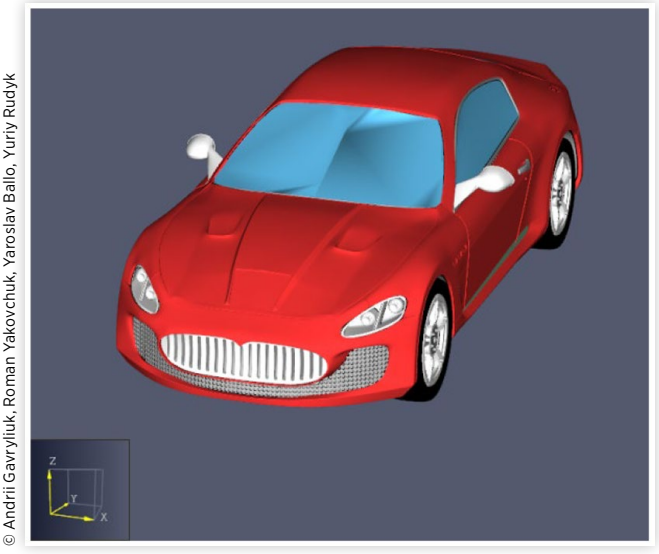

2.3. The Choice of the Location of the Initial Center of the Fire and Its Development

Based on the analysis of references, it was determined that the most common cause of fire in electric vehicles is a short circuit, which causes the cable products to burn. As a result, the thermal effect caused the depressurization of the traction battery with its subsequent ignition. The initial chemical reaction of combustion consists of: C (carbon atoms)—1.9; H (hydrogen atoms)—40.0; O (oxygen atoms)—2.6. The emission of CO is 0.015 and soot is 0.098. There is no reduction in burning intensity (self-extinguishing). The maximum heat capacity of heat release is 5200 kW/m^2 (accepted according to data [55]). The linear speed of flame propagation is 0.21 m/s (taken according to [49, 50]).

According to the adopted scenario, the fire develops freely during the simulation time (720 s). The critical ignition temperature of adjacent materials that are part of the structure of the electric vehicle is taken as the material with the lowest self-ignition temperature, namely 160°C (for synthetic fabrics).

The main task during the development of a mathematical model is the maximum approximation of the parameters of the model to the conditions of the process and interrelationships of objects. In the specified process, the following are involved: distances between objects, linear dimensions of objects, materials of objects, environmental parameters, fire load of objects and their combustion reactions, the scenario of occurrence and continuation of the burning process, and the like.

During the mathematical description of the geometric boundary conditions, the shape and linear dimensions of the research object are set to the scale of the relevant local conditions, and the distance between the research objects is observed.

2.4. Setting Environmental Parameters and Initial Values of Output Parameters

Environmental parameters and initial parameter values are set for both indoors and outdoors. A mathematical model of the development of the fire is also formed, and the dynamics of its development are simulated.

The following assumptions are allowed during the evaluation of fire protection distances by calculation methods:

- The flame temperature is assumed to be the same over the entire surface;
- The temperature of substances or materials that perceive heat from a fire in an adjacent object is assumed to be 20°C at the initial moment of calculation.

When using the simplified calculation method for estimating fire protection distances and the method using the equation of radiant heat exchange and the equation of nonstationary thermal conductivity, the following environmental conditions are assumed:

- Air temperature 20°C, atmospheric pressure 1 atm, wind speed 0 m/s;
- The thermal effect of a fire on an adjacent object is determined due to thermal radiation, the convective component may not be taken into account;
- In the absence of data, the degree of blackness of the flame (ε_f) is taken to be equal to $\varepsilon_f = 1$, and the degree of blackness of the surface of the material or substance that perceives heat from a fire in the adjacent construction object (ε_m) is taken to be equal to $\varepsilon_m = 0.8$, as for wood;
- The cause of the fire is not considered.

During the simulation, the wind effect is not considered, as it decreases the density and uniformity of the heat flow and reduces the height of the fire flame. In addition, the wind toward the building will create support and a zone of increased pressure. In this case, the cold air will enter the heating zone of the facade due to swirling and will accordingly cool the wall of the building.

2.5. Establishing Criteria for Evaluating Results

For calculations, two main fire scenarios have been defined. The first scenario is a fire in the parking lot bordering the wall of the building. The ignition of an electric vehicle in a closed parking lot is considered the second fire scenario. According to the selected scenarios, the criteria for successful or unsuccessful calculations should be accepted.

Given that the building is the main adjacent object of the study in the fire scenario, it is advisable to determine the safety criteria for this object.

At the same time, one of the main reasons for the spread of fire not only along the vertical external enclosing structures but also into the interior of the room is the destruction of the structures filling the light openings, namely windows. Today, as a rule, light openings are filled with metal-plastic windows. Analysis of the construction and types of materials of metal-plastic windows showed that the composition of the windows includes combustible materials. They create prerequisites for the spread of fire inside the premises due to their destruction: plastic (polyvinyl chloride), rubber, aluminum, wood, fiberglass, sealant, as well as combined materials that include the listed. The lowest self-ignition temperature is the sealant, which is a polymer composition and swells at a temperature of 150°C and ignites at a temperature of 210–230°C. The plastic seal-lock of double-glazed windows, which does not have a metal frame and is easily deformed under the influence of temperatures starting from 250°C, is also a fire hazard. Taking into account the analysis of the most resonant fires for open

parking lots [49], it was found that the greatest thermal radiation for open space was observed from an electric car placed near a brick wall without light slots; during the creation of the model, this scenario was adopted.

Thus, the maximum temperature value of 120°C on the building wall was adopted as the safety criterion. This criterion is used to determine the safe fire distance in order to restrict the propagation of fire along the external enclosing structures of the building. It also serves to substantiate the safety of utilizing facade system materials through the analysis of various methods [60].

Therefore, in order to establish a safe distance to prevent the spread of fire along the external structures of the building and validate the safety of facade system materials using various analytical methods, a safety criterion was established. This criterion sets the maximum temperature value on the building wall at 120°C.

3. Research Results and Their Discussion

Based on the results of the simulation of the study of safe fire distances, geometric models of the electric car and a fragment of a solid wall of an adjacent building was created. The electric car is a simulated source of thermal radiation, and the wall is subject to thermal radiation and is an object on which temperature values are directly measured. In Figure 3 a fragment of the model with a corner wall is given.

For the possibility of visual evaluation of thermal distributions, the external surface of the facade provides the possibility of visualization of the temperature change of the surface heating during the entire duration of the simulation.

In order to determine the specific values of the spread of the upward heat flow during a fire in an electric car, heat meters in a gas medium are arranged from its center and in each direction with a step of 50 cm.

Thermal meters that are located in front of the electric vehicle are marked with the letter F, those located on the left L, on the right R, and those behind. The numerical value next to the marking indicates the distance of the thermal meter from the electric vehicle in meters.

These meters will record the change in temperature values in the volume of air space between the body of the electric vehicle and the building. Figure 4 shows the appearance of the model and the location of the meters in the gas environment.

Based on the simulation results, temperature distributions and heat exchange between adjacent objects during an electric vehicle fire is determined. The average HRR during the burning of LIB is about 3 MW for up to 12 minutes from the start of the fire test. Thus, the created model made it possible to reproduce the rate of heat release during the study of the combustion processes of LIB in electric vehicles, which is shown in Figure 5.

Dangerous factors of fire, namely smoke, combustion products, and heat, spread freely from the center of the fire. A series of tests were carried out step by step with a step of increasing the distance by 0.5 m from the wall to the electric vehicle. The tests were carried out until a safe fire distance from the electric car to the wall was determined, at which the thermal distribution on it would not exceed 120°C.

The most common and simplest (in terms of fire safety) scenario for modeling an electric vehicle fire. Other scenarios can complicate the model and worsen fire safety parameters (fire protection distance, etc.). The "minimum fire protection distance" is applied as the distance from the fire site to building structures or other parked vehicles. The word

FIGURE 3 A fragment of the created model of an open parking lot with a corner wall.

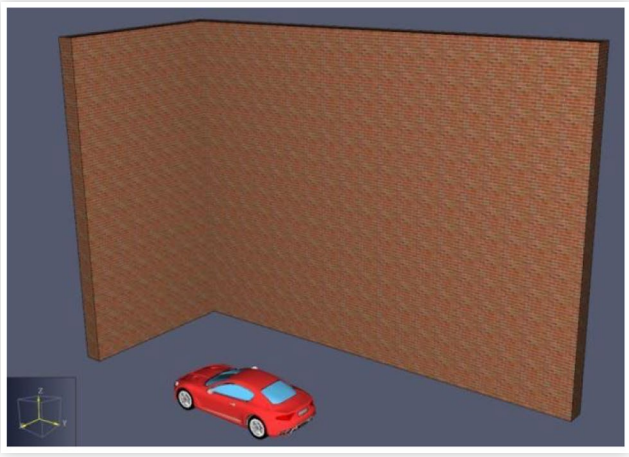

FIGURE 4 A fragment of the created model of an open parking lot with a corner wall and meters in the gas phase.

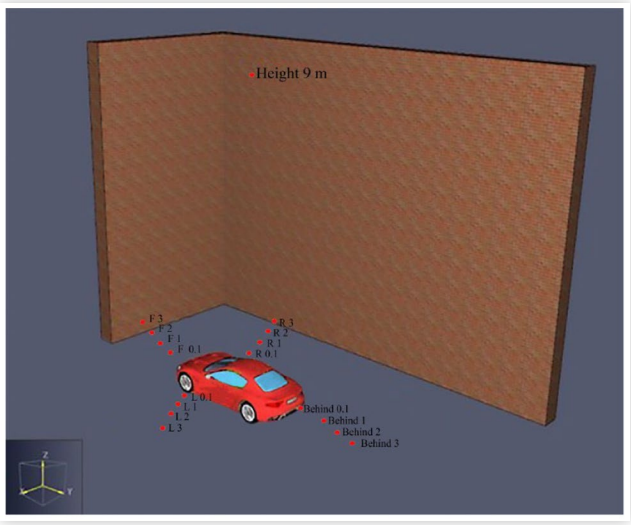

FIGURE 5 Reproduced mode of the rate of heat release during the study of combustion processes of an electric vehicle with a traction lithium-ion battery.

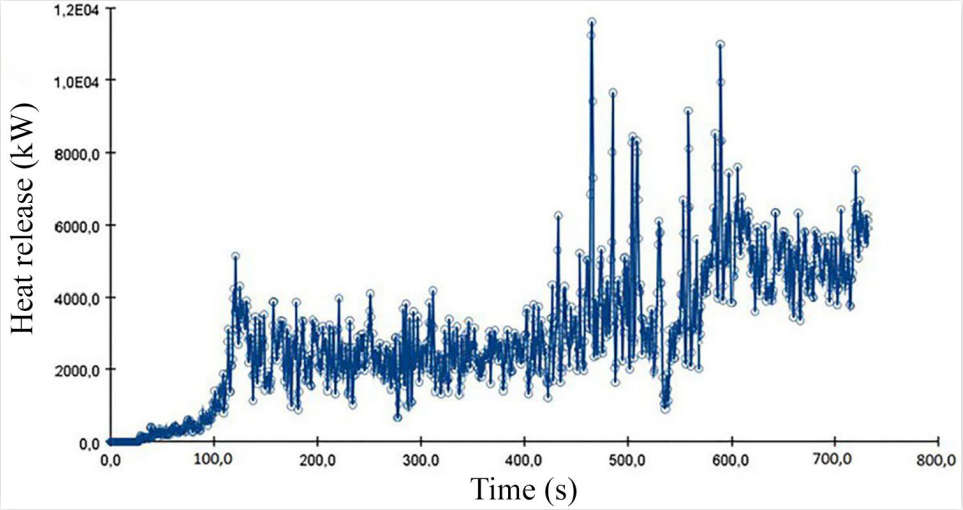

"minimum" of fire protection distance refers to the initial conditions of safety design (Figure 6).

The results of displaying the dynamics of fire spread and changes in thermal distribution in space over time are presented in Figures 7–11.

According to the simulation results, it was determined that the fire-fighting distance from the electric charging point and the electric car to the wall of buildings of various functional purposes should be at least 3 m. The obtained data on the safe fire-fighting distance will prevent the spread of fire from the electric car both along the facade system of the building and into the interior of the room through light slits.

This fire separation distance was obtained for the given conditions of an electric vehicle fire. It is safe to assume that fires caused by different electric vehicle types, such as electric trucks, are capable of producing higher thermal emissions and heat fluxes. As such, the fire protection distance will be much greater than 3 m. On the other hand, in this study, the critical temperature on the parking lot wall was assumed to be 120°C. If the parking lot wall is deemed to withstand temperatures exceeding 120°C, the fire separation distance will be much smaller.

4. Conclusions

In this study, using the FDS, a BEV fire was simulated using the Tesla Model S car as an example. Based on literature analysis and known data on the heat of combustion of the materials that make up the car, as well as field test data by the authors Sungwook Kang and others [46] the FDS model of the Tesla Model S electric car was created.

Taking into account that the average time of arrival of fire and rescue units is up to 10 minutes, and approximately up to 2 minutes for the supply of fire extinguishing agents,

FIGURE 6 A fragment of the simulation of the extreme temperature distribution of 120°C on the adjacent wall at a distance of 3 m.

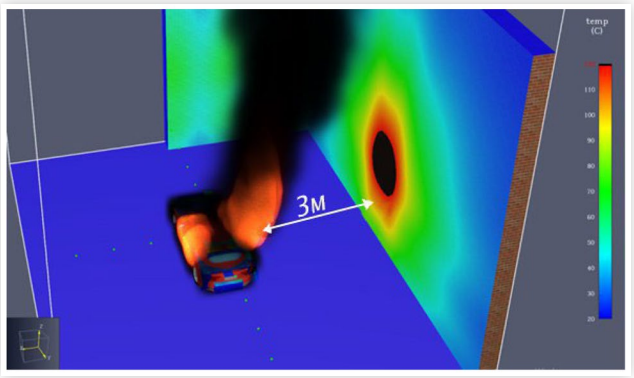

FIGURE 7 A fragment of the simulation of fire development at 60 s.

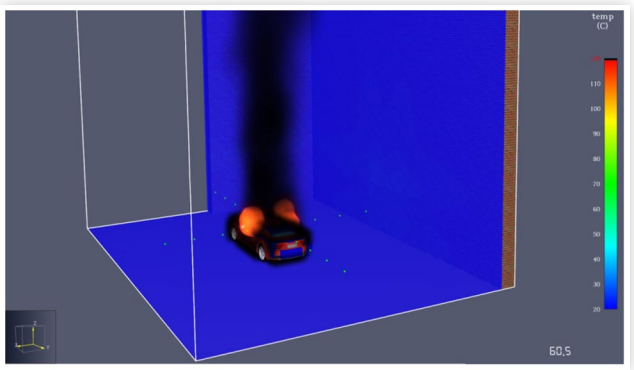

FIGURE 8 A fragment of the simulation of fire development at 180 s.

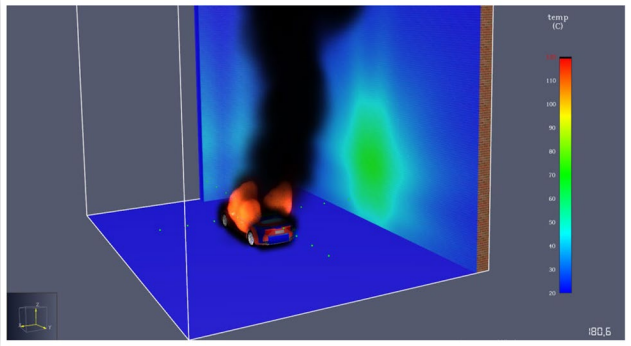

FIGURE 9 A fragment of the simulation of fire development at 400 s.

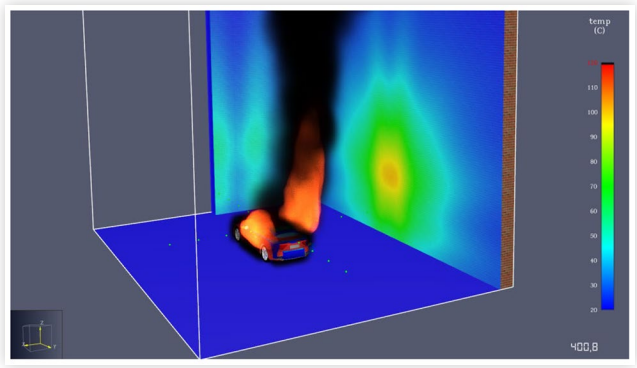

FIGURE 10 A fragment of the simulation of fire development at 600 s.

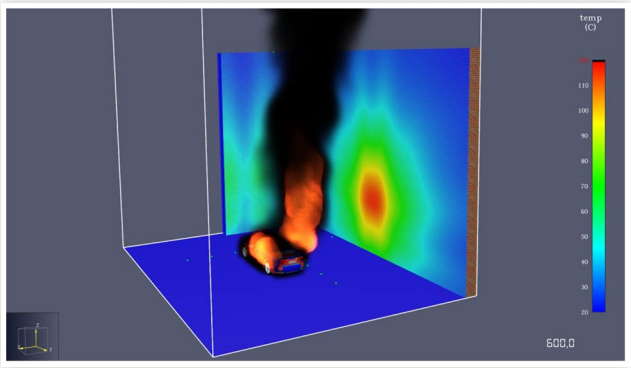

FIGURE 11 A fragment of the simulation of fire development and thermal distributions on the wall at 720 s of the fire.

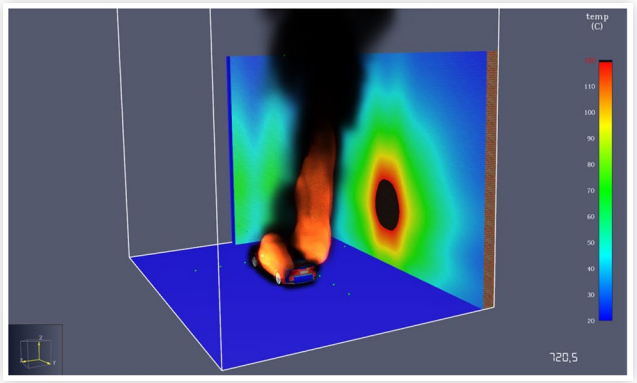

therefore the time of 12 minutes, that is, 720 s, became the simulation time of the Tesla Model S fire.

Tesla Model S fire modeling was carried out with the aim of determining a safe fire-fighting distance to ensure the limitation of the spread of fire along the external enclosing structures of the building and to justify the safety of the use of facade system materials based on the analysis of methods [56] the safety criterion of not exceeding the maximum temperature value of 120°C for the wall of the building.

Based on the results of the simulation of the study of safe fire distances, geometric models of the electric car and a fragment of a solid wall of an adjacent building were created. The electric car is a simulated source of thermal radiation, and the wall is subject to thermal radiation and is an object on which temperature values are directly measured. During modeling, it is allowed to adapt the building wall material to specific conditions. This makes it possible to adjust the minimum fire protection distance.

On the basis of modeling, it was determined that taking into account the safety criterion of a temperature value of 120°C on the wall of the building and the time of free fire development of 600 s, the minimum fire-fighting distance from the electric vehicle to the wall of buildings of various functional purposes should be 3 m.

Further research should be focused on modeling the development of a fire and its extinguishing by firefighters. Realizing such an idea causes certain difficulties, as it is necessary to adhere to the amount of supply and type of fire extinguishing agent, which can vary dramatically depending on the fire brigade.

Declaration of Competing Interest

The authors declare that they have no known competing financial interests or personal relationships that could have appeared to influence the work reported in this article.

Contact Information

Andrii Gavryliuk
corresponding author
Candidate of Technical Sciences, Associate Professor, The Full-Time Doctoral Student of the Doctoral Program
Lviv State University of Life Safety
Lviv, 79000 Ukraine
Gavrilyk3@gmail.com

Roman Yakovchuk
Doctor of Technical Science, Associate Professor, Head of the Department of Civil Protection and Computer Modeling Ecology-Geophysical Processes
Lviv State University of Life Safety
35 Kleparivska str., Lviv, 79000 Ukraine
yakovchukrs@ukr.net

Yaroslav Ballo
Candidate of Technical Sciences, Deputy Head of the Regulatory Technical Support Department of the Fire Protection Research Center
The Institute of Public Administration and Research in Civil Protection
Kyiv, 79000 Ukraine
2801397@ukr.net

Yuriy Rudyk
Doctor of Technical Science, Associate Professor Department of Research and Development
Lviv State University of Life Safety
Lviv, Ukraine Lviv, 79000 Ukraine
rudra@ukr.net

References

1. Chan, C.C. and Wong, Y.S., "Electric Vehicles Charge Forward," *IEEE Power and Energy Magazine* 2, no. 6 (2004): 24-33.
2. Matulka, R., "The History of the Electric Car," Department of Energy, accessed 10 March 2023, https://www.energy.gov/articles/history-electric-car.
3. International Energy Agency, "Global EV Outlook, 2022: Securing Supplies for an Electric Future; 2022 IIS 2380-S43," 2022, accessed 12 March 2023, https://statistical.proquest.com/statisticalinsight/result/pqpresultpage.previewtitle?docType=PQSI&titleUri=/content/2022/2380-S43.xml.
4. Willstrand, O., Bisschop, R., Blomqvist, P., Temple, A. et al., "Toxic Gases from Fire in Electric Vehicles," 2020.
5. Zhang, Z.J., Ramadass, P., and Fang, W., "Safety of Lithium-Ion Batteries," in *Lithium-Ion Batteries* (Elsevier, 2014), 409-435.
6. Fire, A.P.U.B., "Japan Airlines Boeing 787-8, JA829J," NTSB/AIR-14/01, National Transportation Safety Board, Boston, MA, 2014.
7. Goto, N., "Aircraft Serious Incident Investigation Report: All Nippon Airways Co. Ltd. JA804A," Rep. No. AI2014-4, Japan Transport Safety Board, Tokyo, Japan, September 25, 2014.
8. Gavryliuk, A.F. and Kushnir, A.P., "Analysis of Fire Danger of Electric Vehicles according to Thermal Stability of Powerful Lithium Battery," *Fire Safety* 40 (2022): 31-39, doi:https://doi.org/10.32447/20786662.40.2022.04.
9. Extremetech, "Tesla Model S Catches Fire at Supercharger Station in Norway," accessed 12 March 2023, https://www.extremetech.com/extreme/220237-tesla-model-s-catches-fire-at-supercharger-station-in-norway.
10. Kim, Y.H., "How to Resolve Electric Vehicle Fires," Fire Protection News, National Fire Research Institute of Korea, accessed 14 March 2023, https://www.fpn119.co.kr/171590.
11. Autoblog, "Tesla Model S Catches Fire Near Seattle, No Injuries Reported," 2013, accessed 16 March 2023, https://www.autoblog.com/2013/10/02/tesla-model-s-fire/.
12. Hainan, "A New Energy Bus Crashed into a Guardrail and Caught Fire in Wanning, Fortunately Causing No Casualties," 2020, accessed 18 March 2023, http://hainan.sina.com.cn/news/hnyw/2020-11-26/detail-iiznctke3332328.shtml?from=hainan_ydph.
13. BahooToroody, F., Khalaj, S., Leoni, L., De Carlo, F. et al., "Reliability Estimation of Reinforced Slopes to Prioritize Maintenance Actions Bahootoroody," *International Journal of Environmental Research and Public Health* 18, no. 2 (2021): 373.
14. Di Bona, G., Falcone, D., and Forcina, A., "AHP-TOPSIS Model to Evaluate Maintenance Strategy Using RAMS and Production Parameters," *International Journal of Operations and Quantitative Management* 25, no. 3 (2019): 175-201.
15. Schmidt, A., Oehler, D., Weber, A., Wetzel, T. et al., "A Multi Scale Multi Domain Model for Large Format Lithium-Ion Batteries," *Electrochimica Acta* 393 (2021): 139046.
16. Chen, M., Sun, Q., Li, Y., Wu, K. et al., "A Thermal Runaway Simulation on a Lithium Titanate Battery and the Battery Module," *Energies* 8, no. 1 (2015): 490-500.
17. Wu, W., Xiao, X., and Huang, X., "The Effect of Battery Design Parameters on Heat Generation and Utilization in a Li-Ion Cell," *Electrochimica Acta* 83 (2012): 227-240.
18. Abada, S., Marlair, G., Lecocq, A., Petit, M. et al., "Safety Focused Modeling of Lithium-Ion Batteries: A Review," *Journal of Power Sources* 306 (2016): 178-192.
19. Anderson, J., Larsson, F., Andersson, P., and Mellander, B.E., "Thermal Modeling of Fire Propagation in Lithium-Ion Batteries," in *Proceedings of the 24th International Technical Conference on the Enhanced Safety of Vehicles (ESV)*, Gothenburg, Sweden, 8-11, 2015.
20. Anderson, J., Sjöström, J., Andersson, P., Amon, F. et al., "Experimental and Numerical Characterization of an Electrically Propelled Vehicles Battery Casing Including Battery Module," *Journal of Thermal Science and Engineering Applications* 6, no. 4 (2014): 041015.
21. Zhao, W., Luo, G., and Wang, C.Y., "Modeling Nail Penetration Process in Large-Format Li-Ion Cells," *Journal of the Electrochemical Society* 162, no. 1 (2014): A207.
22. Henriksen, M., Vaagsaether, K., Lundberg, J., Forseth, S. et al., "Simulation of a Premixed Explosion of Gas Vented during Li-Ion Battery Failure," *Fire Safety Journal* 126 (2021): 103478.

23. Larsson, F., Anderson, J., Andersson, P., and Mellander, B.E., "Thermal Modelling of Cell-to-Cell Fire Propagation and Cascading Thermal Runaway Failure Effects for Lithium-Ion Battery Cells and Modules Using Fire Walls," *Journal of the Electrochemical Society* 163, no. 14 (2016): A2854.
24. Truchot, B., Leroy, G., and Marlair, G., "CFD and Engineering Method Coupling for Evaluating the Fire Relative to Battery Transportation," in *8th International Conference on Tunnel Safety and Ventilation*, Graz, Austria, 132-140, April 2016.
25. Hatchard, T.D., MacNeil, D.D., Basu, A., and Dahn, J.R., "Thermal Model of Cylindrical and Prismatic Lithium-Ion Cells," *Journal of the Electrochemical Society* 148, no. 7 (2001): A755.
26. Baba, N., Yoshida, H., Nagaoka, M., Okuda, C. et al., "Numerical Simulation of Thermal Behavior of Lithium-Ion Secondary Batteries Using the Enhanced Single Particle Model," *Journal of Power Sources* 252 (2014): 214-228.
27. Gudym, V., Mykhalichko, B., Nazarovets, O., and Gavryliuk, A., "The Effect of Short Circuits and Flame Temperature Modes on the Change in the Microstructure of Copper in Automotive Wiring," *Engineering Failure Analysis* 136 (2022): 106198.
28. Zhang, B., Lu, Z., Liu, Z., Liang, G. et al., "Investigation of a Vehicle Fire Caused by Manufacturing Defect," *Engineering Failure Analysis* 91 (2018): 28-34.
29. Xiao, M. and Choe, S.Y., "Theoretical and Experimental Analysis of Heat Generations of a Pouch Type $LiMn_2O_4$/Carbon High Power Li-Polymer Battery," *Journal of Power Sources* 241 (2013): 46-55.
30. Arora, S. and Kapoor, A., "Experimental Study of Heat Generation Rate during Discharge of $LifePO_4$ Pouch Cells of Different Nominal Capacities and Thickness," *Batteries* 5, no. 4 (2019): 70.
31. Rashidi, S., Karimi, N., Sunden, B., Kim, K.C. et al., "Progress and Challenges on the Thermal Management of Electrochemical Energy Conversion and Storage Technologies: Fuel Cells, Electrolysers, and Supercapacitors," *Progress in Energy and Combustion Science* 88 (2022): 100966.
32. Liu, B., Zhang, J., Zhang, C., and Xu, J., "Mechanical Integrity of 18650 Lithium-Ion Battery Module: Packing Density and Packing Mode," *Engineering Failure Analysis* 91 (2018): 315-326.
33. Voigt, S., Sträubig, F., Kwade, A., Zehfuß, J. et al., "An Empirical Model for Lithium-Ion Battery Fires for CFD Applications," *Fire Safety Journal* 135 (2022): 103725.
34. Xia, Y., Chen, G., Zhou, Q., Shi, X. et al., "Failure Behaviours of 100% SOC Lithium-Ion Battery Modules under Different Impact Loading Conditions," *Engineering Failure Analysis* 82 (2017): 149-160.
35. Wang, Y.W. and Shu, C.M., "Energy Generation Mechanisms for a Li-Ion Cell in Case of Thermal Explosion: A Review," *Journal of Energy Storage* 55 (2022): 105501.
36. Feng, X., Ouyang, M., Liu, X., Lu, L. et al., "Thermal Runaway Mechanism of Lithium Ion Battery for Electric Vehicles: A Review," *Energy Storage Materials* 10 (2018): 246-267.
37. Okamoto, K., Watanabe, N., Hagimoto, Y., Chigira, T. et al., "Burning Behavior of Sedan Passenger Cars," *Fire Safety Journal* 44, no. 3 (2009): 301-310.
38. Watanabe, N., Sugawa, O., Suwa, T., Ogawa, Y. et al., "Comparison of Fire Behaviors of an Electric-Battery-Powered Vehicle and Gasoline-Powered Vehicle in a Real-Scale Fire Test," in *Proceedings from 2nd International Conference on Fires in Vehicles-FIVE*, Chicago, IL, 195-206, September 2012.
39. Mohd Tohir, M.Z. and Spearpoint, M., "Distribution Analysis of the Fire Severity Characteristics of Single Passenger Road Vehicles Using Heat Release Rate Data," *Fire Science Reviews* 2, no. 1 (2013): 1-26.
40. Chattaway, A., Dunster, R., Weller, P., and Peoples, J., "The Development of a Standard Test for Assessing the Effectiveness of Transit Vehicle Fire Extinguishing Systems," *SAE Int. J. Commer. Veh.* 5, no. 1 (2012): 354-363, doi:https://doi.org/10.4271/2012-01-0986.
41. Smith, P., Chattaway, A., and Peoples, J., "A Comparison of Various Fire Detection Methodologies in Transit Vehicle Fire Protection Systems," *SAE Int. J. Commer. Veh.* 5, no. 1 (2012): 343-353, doi:https://doi.org/10.4271/2012-01-0983.
42. Lecocq, A., Bertana, M., Truchot, B., and Marlair, G., "Comparison of the Fire Consequences of an Electric Vehicle and an Internal Combustion Engine Vehicle," in *2nd International Conference on Fires in Vehicles—FIVE 2012*, Chicago, IL, 183-194, September 27–28, 2014.
43. Lam, C., MacNeil, D., Kroeker, R., Lougheed, G. et al., "Full-Scale Fire Testing of Electric and Internal Combustion Engine Vehicles," in *4th International Conference on Fire in Vehicles*, Baltimore, MD, October 5–6, 2016.
44. Sun, P., Huang, X., Bisschop, R., and Niu, H., "A Review of Battery Fires in Electric Vehicles," *Fire Technol* 56 (2020): 1361-1410.
45. Matsumura, H., Itoh, S., Matsushima, K., and Okada, T., "Temperature Characteristics of a Hybrid Electric Vehicle Fire," *SAE Int. J. Alt. Power.* 1, no. 1 (2012): 195-207, doi:https://doi.org/10.4271/2012-01-0982.
46. Kang, S., Kwon, M., Choi, J.Y., and Choi, S., "Full-Scale Fire Testing of Battery Electric Vehicles," *Applied Energy* 332 (2023): 120497.
47. Willstrand, O., Bisschop, R., Blomqvist, P., Temple, A. et al., "Toxic Gases from Fire in Electric Vehicles," RISE Report 2020: 90, 2020.
48. Sturm, P., Fößleitner, P., Fruhwirt, D., Galler, R. et al., "Fire Tests with Lithium-Ion Battery Electric Vehicles in Road Tunnels," *Fire Safety Journal* 134 (2022): 103695.
49. McGrattan, K. et al., "Fire Dynamics Simulator (Version 5) Technical Reference Guide Volume 1: Mathematical Model," NIST Special Publication 1018-5, 2009.
50. McGrattan, K. et al., "Fire Dynamics Simulator (Version 5) User's Guide," NIST Special Publication 1019-5, 2009.
51. ISO, "Fire Safety Engineering—Procedures and Requirements for Verification and Validation of Calculation

Methods—Part 1: General," ISO 16730-1:2015, 2015, accessed 23 March 2023, https://www.iso.org/standard/62111.html.

52. Forney, G.P., "Smokeview (Version 5): A Tool for Vizualizing Fire Dynamics Simulation Data Volume 1: User's Guide," NIST Special Publication 1017-1, 2008.
53. Tatsii, R.M., Stasyuk, M.F., and Pazen, O.Y., "Direct Method of Calculating Nonstationary Temperature Fields in Bodies of Basic Geometric Shapes," *Journal of Engineering Physics and Thermophysics* 94, no. 2 (2021): 298-310, doi:10.1007/s10891-021-02302-z.
54. Electrek, "Tesla Says Model S Fire in France Was due to 'Electrical Connection Improperly Tightened' by a Human Instead of Robots," September 9, 2016, accessed 25 March 2023, https://electrek.co/2016/09/09/tesla-fire-france-electrical-connectionimproperly-tightened-human-robot/.
55. RISE, "Toxic Gases from Fire in Electric Vehicles," RISE Rapport 2020:90, 2020, accessed 29 March 2023, http://ri.diva-portal.org/smash/get/diva2:1522149/FULLTEXT01.pdf.
56. Emilsson, E. and Dahllöf, L., "Plastics in Passenger Cars—A Comparison Over Types and Time," 2019.
57. Bhunia, P.R., Gupta, S., Garg, A., and Gupta, R.K., *Specialty Polymers* [online] (Boca Raton, FL: CRC Press, 2022), accessed 10 April 2023, doi:https://doi.org/10.1201/9781003278269.
58. Modi, S. and Vadhavkar, A., "Technology Roadmap: Materials and Manufacturing," Center for Automotive Research, Ann Arbor, MI, 2019.
59. Bhuwalka, K., Field, F.R. III, De Kleine, R.D., Kim, H.C. et al., "Characterizing the Changes in Material Use due to Vehicle Electrification," *Environmental Science & Technology* 55, no. 14 (2021): 10097-10107.
60. Chu, F., Yamaoka, T., Ide, H., and Kimura, Y., "Microvoid Formation Process during the Plastic Deformation of β-Form Polypropylene," *Polymer* 35, no. 16 (1994): 3442-3448.